01 Jan 2023

PtCo/MWCNTs Prepared By A Microwave-assisted Polyol Method For Selective Cinnamaldehyde Hydrogenation

Kaiying Wang

Yuzi Liu

Jee-Ching Wang
Missouri University of Science and Technology, jcwang@mst.edu

Xinhua Liang
Missouri University of Science and Technology, liangxin@mst.edu

Recommended Citation

PtCo/MWCNTs Prepared by a Microwave-assisted Polyol Method for Selective Cinnamaldehyde Hydrogenation

Kaiying Wang,[a] Yuzi Liu,[b] Jee-Ching Wang,[c] and Xinhua Liang*[a]

Abstract: Using microwave irradiation, PtCo alloy nanoparticles were deposited within a few minutes on COOH-functionalized MWCNT supports. The obtained catalysts were used for selective hydrogenation of cinnamaldehyde, a reaction whose products are widely used in various fields. In the selective cinnamaldehyde hydrogenation to cinnamyl alcohol, microwave-prepared catalysts (generically, Pt_xCo_y-MW) outperformed a catalyst prepared by the conventional method (Pt_1Co_2-con). The highest selective hydrogenation to cinnamyl alcohol, 89%, was obtained using Pt_1Co_2-MW, while Pt_1Co_2-con showed a selectivity of 76%. Characterization results confirmed that the microwave prepared samples had a stronger interaction between Pt and Co than that in the Pt_1Co_2-con sample. The alloyed Co altered the electronic structure of Pt, leading to favorable adsorption of the $C{=}O$ bond by the lone-pair electrons of its oxygen atom. Moreover, the Pt_1Co_2-MW sample showed neglectable change in catalytic performance (e. g., cinnamaldehyde conversion and selective hydrogenation to cinnamyl alcohol) during recycling experiments.

Introduction

Bimetallic catalysts have received increasing attention in recent decades because of their enhanced selectivity, activity, and stability compared with their parent counterparts.[1] These unexpected properties make bimetallic catalysts an interesting class of materials in many catalytic[2–3] and electrocatalytic processes.[4] This work focuses on alloyed nanoparticles (NPs) because they can be easily obtained using standard catalyst preparation methods and allow easy tuning of their catalytic properties by varying their compositions. Alloying also can result in new properties arising from alloying effects, providing potential advantages over monometallic catalysts. Because of their excellent performance, Pt-based alloys have been investigated extensively in various areas.[1] For example, owing to the enhanced electronic interactions, Pt–M (M=Fe, Co, Ni, or Cu) alloys exhibited superior activity in oxygen reduction reaction (ORR).[5–7] PtCo alloy showed exceptional catalytic efficiency in selectively hydrogenating α,β-unsaturated aldehydes, correlating with the synergistic effect between Pt and Co.[8–9]

The key is to prepare Pt-alloys with controlled sizes, morphologies, and compositions. Most reported methods employ stabilizing ligands[10–12] or surfactants[13] to control the particle size of the Pt-alloys. However, challenges remain with these methods. Capped ligands or surfactants can block active sites or even change the chemoselectivity and enantioselectivity of the reactions.[10] Surfactants, such as polyvinyl pyrrolidone, have restricted use in preparation of electrocatalysis because metal particles severely agglomerate after removal of the surfactant at relatively high temperatures.[14] Although other methods, such as impregnation, sol-gel, and co-precipitation, have been developed, these processes usually generate large amounts of waste solvents, and the prepared alloys easily aggregate.[9] Thus, to overcome these challenges, a green and effective method for preparing well-defined alloys is needed.

Polyol synthesis, in which polyols act as both solvent and reducing agent,[14] is very promising for this purpose because it uses minimal raw material. Moreover, polyol can coordinate with metal precursors as well as with the particle surface, thus minimizing coalescence. The high viscosity of polyol facilitates a diffusion-controlled regime for particle growth, which yields a controlled structure and morphology.[15] Typically, polyol synthesis is conducted at temperatures above 150 °C to allow metallic ion reduction by the polyol, and the preparation temperature depends on the choice of solvent. Traditionally, at laboratory scale the required high temperature conditions are achieved by conduction heating using a hotplate. But conduction heating is inefficient and slow, requiring a long period of temperature increase to reach the target temperature, during which time temperature gradients tend to form across the reactant mixture. Microwave (MW) heating is an alternative that has emerged in the past two decades in the field of nanomaterial synthesis and chemical transformations, and it offers many benefits over conventional heat treatments, such as very high temperature ramp-up rates and minimal thermal gradients.[16]

It is generally accepted that the formation of homogeneous colloidal particles is aided by the uniform growth of nanoparticles. Concentration and temperature gradients should be

[a] K. Wang, Prof. Dr. X. Liang
Department of Energy, Environmental & Chemical Engineering,
Washington University in St. Louis,
St. Louis, MO 63130 (United States)
E-mail: Xinhua.Liang@wustl.edu

[b] Dr. Y. Liu
Center for Nanoscale Materials, Argonne National Laboratory,
Argonne, IL 60439 (United States)

[c] Prof. Dr. J.-C. Wang
Linda and Bipin Doshi Department of Chemical
and Biochemical Engineering,
Missouri University of Science and Technology,
Rolla, MO 65409 (United States)

avoided to provide a favorable environment for homogeneous growth. In contrast to conventional heating, MW-assisted heating can reach a maximum reaction temperature within a few seconds.[17] Accordingly, MW technology has been widely applied in polyol synthesis.[18] Importantly, alloys obtained with MW heating have better controlled structures as well as better catalytic performance and stability than those obtained with conventional heating.[19–21] For example, carbon supported PtY alloy prepared in ethylene glycol (EG) under MW heating exhibited higher ORR activity than catalysts prepared by using traditional heating methods and heat treatment under a H_2/Ar or Ar atmosphere.[22] In other research, MW-assisted fabrication of Pt_3Co alloy on reduced graphene oxide demonstrated higher metal utilization and dispersion than the conventional heating method.[9] The obtained Pt_3Co alloy was extremely active and selective during the hydrogenation of cinnamaldehyde (CAL) to cinnamyl alcohol (COL). In a recent report, PtRu alloy on MWCNTs prepared with MW outperformed PtRu/MWCNT samples prepared by other synthesis methods in the methanol electro-oxidation reaction.[23] Moreover, PtRu/MWCNT catalyst prepared with MW heating showed better stability under high current density than the same catalyst obtained by other methods.

In this study, the MW-assisted polyol method was used to prepare PtCo alloys. EG was chosen as the solvent because of its high dielectric constant (41.4 at 25 °C) and high dielectric loss.[14] The selective hydrogenation of CAL was chosen to evaluate the performance of the prepared catalysts. CAL provides C=C and C=O bonds, so two competing reaction pathways can be followed: either selective conversion of the aldehyde to the corresponding unsaturated alcohol or a thermodynamically more favorable reduction of the olefin bond.[24–25] The optimized Pt_1Co_2-MW catalyst exhibited high activity and selectivity in converting CAL to COL, as well as high stability. A series of characterizations revealed that the superb performance came from the strong interaction between Pt and Co.

Results and discussion

Characterization of PtCo catalysts

As shown in Figure 1, the XRD patterns of all the samples showed typical Pt face-centered cubic (FCC) features. For the Pt-MW sample, the diffraction peaks at around 26° and 43° were attributed to the (002) and (101) planes of the MWCNTs, respectively.[26] The other four diffraction peaks, at 39.9°, 46.4°, 67.6°, and 81.5°, were consistent with those of pure Pt metals with an FCC structure, corresponding to the (111), (200), (220), and (311) planes, respectively.[27] For the Pt_xCo_y-MW samples, no crystalline structure of Co was observed, while the characteristic diffraction peaks of Pt were still observed, with a positive shift in the 2θ value, compared with the Pt-MW sample. The absence of diffraction peaks typical of Co can be attributed to the Co being dissolved in a Pt lattice, in other words, forming a PtCo alloy.[28] As shown in Table S1, the lattice parameters of the
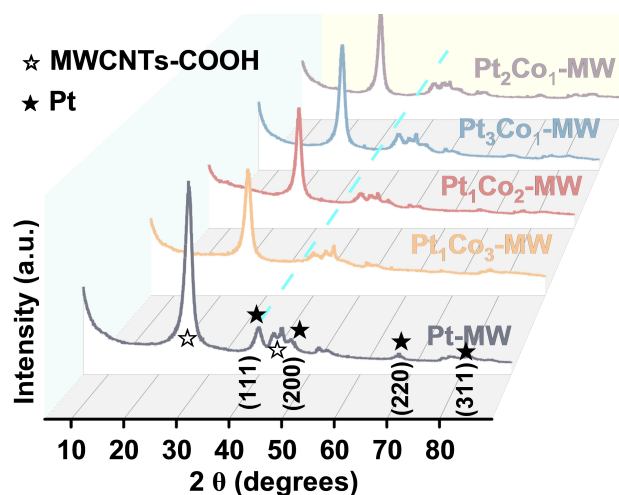
Figure 1. XRD patterns of Pt-MW and Pt_xCo_y-MW catalysts.

Pt_xCo_y-MW samples were found to be lower than that of the Pt-MW sample, further indicating that Co was incorporated into the Pt FCC structure to form an alloy phase with a concomitant lattice contraction. Moreover, the intensity of the diffraction peaks for Pt (111) became weaker with the incorporation of Co, so inaccuracy could have been introduced if we had used the Scherrer equation to calculate the particle size. It was more reliable to investigate the particle size distribution with TEM imaging.

The morphology of the catalysts was investigated by STEM-HAADF. Metal species can be clearly observed in HAADF micrographs due to their higher atomic number than the carbon support. As shown in Figure 2, both Pt and PtCo alloy nanoparticles were well dispersed on the surface of the MWCNTs, with average particle sizes of 8.1 ± 1.7 nm and 8.5 ± 1.7 nm, respectively. The bimetallic PtCo was slightly larger than the Pt, due to the alloying of two elements. The large particle size, higher than that reported by other researchers, probably resulted from the high energy of MW heating causing aggregation and particle growth. To confirm the incorporation of Co, the elemental distributions of Co and Pt were measured by EDS mapping. As shown in Figure 2e and 2f, both Pt and Co are well distributed in the PtCo alloy sample, with no obvious phase segregation.

Figure 3 shows the reducibility of the catalysts, as determined by H_2-TPR. No peak for Pt(II) reduction was observed in any of the samples in the tested temperature range, since Pt(II) on the carbon support was easily reduced at temperatures below 100 °C.[24,29–30] For the Pt-MW sample, only a broad peak centered at 600 °C is observed, which can be ascribed to the gasification of MWCNTs.[31] The gasification of MWCNTs occurred with all the samples, happening at a lower temperature for the PtCo samples. The introduced Co may have catalyzed the gasification of carbon material, lowering the reduction temperature of carbon.[32] The PtCo samples prepared with different methods possessed different redox behaviors. The quantitative results of H_2-TPR for PtCo samples are listed in
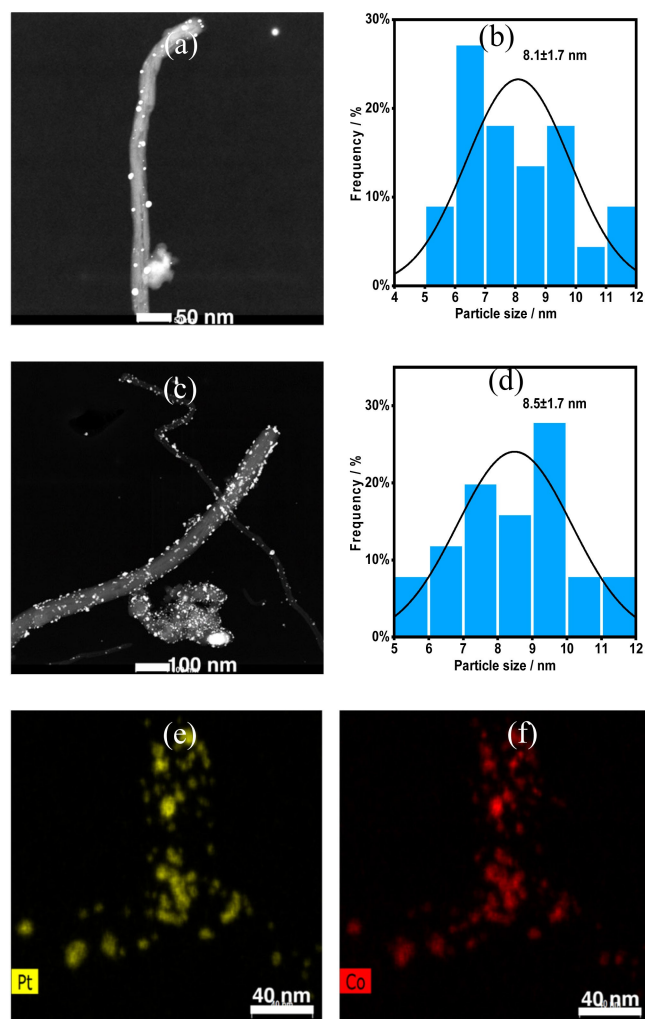
Figure 2. HAADF images of (a) Pt-MW and (b) Pt particle size distribution; HAADF images of (c) Pt$_1$Co$_2$-MW and (d) PtCo particle size distribution; EDS mapping of (e) Pt and (f) Co in Pt$_1$Co$_2$-MW.

to the reduction of CoO to metallic Co^0.[32] According to Table S2, most of the hydrogen was consumed in the reduction of CoO to metallic Co^0. In contrast, for the MW prepared sample Pt$_1$Co$_2$-MW, only one peak was observed, centered at 365 °C and attributed to the reduction of CoO to metallic Co^0. The reduction temperatures of CoO to metallic Co^0 in Pt$_1$Co$_2$-con and Pt$_1$Co$_2$-MW were much lower than that in Co-MWCNTs. As reported previously, the reduction of CoO to Co^0 on MWCNTs occurred at 574 °C.[33] Here, with the hydrogen spillover effect of Pt species, the reduction temperature of CoO to metallic Co^0 was lowered by more than 200 °C for the PtCo samples. Pt$_1$Co$_2$-MW showed a more significant drop in reduction temperature, indicating a stronger interaction between Pt and Co than that in the Pt$_1$Co$_2$-con sample.

The actual metal loading was determined by ICP-OES, and the surface composition was determined by XPS. The nominal values and the actual values are listed in Table 1. Obviously, because of its higher vapor pressure, Co(acac)$_3$ was much more easily reduced than Pt(acac)$_2$, consistent with previous research.[34] For example, almost all Co(acac)$_3$ was reduced, while only ~48% of Pt(acac)$_2$ was reduced by 10 min of MW heating at 197 °C for the Co and Pt monometallic catalysts, respectively. In the PtCo alloy samples, the actual Pt/Co molar ratios were always lower than the nominal ones, due to the easier reduction of Co precursor. Especially for the Co$_{10}$Pt$_2$ and Co$_{10}$Pt$_{10}$ samples, where the Co precursor was first reduced for 10 min, the actual Pt/Co molar ratios were only 0.26 and 0.38, respectively. These values were much lower than the calculated ratio value based on the amount of precursors (i.e., 0.50). The actual Pt/Co molar ratio was closer to the theoretical value, with higher Co content. For example, the actual Pt/Co molar ratio in Pt$_1$Co$_3$-MW was 97% of its nominal value, while that in Pt$_3$Co$_1$-MW was only 55% of its nominal value. Moreover, the coexistence of Co(acac)$_3$ boosted the reduction of Pt(acac)$_2$. Compared with the ~48% reduction of Pt(acac)$_2$ in Pt-MW, 93% of Pt(acac)$_2$ was reduced in Pt$_1$Co$_3$-MW. The other PtCo samples also showed higher reduction efficiencies of Pt(acac)$_2$ with the addition of Co(acac)$_3$. One possible explanation was that the generated Co^0 could have catalyzed the reduction of Pt(acac)$_2$ and Co(acac)$_3$, as reported by Kwon et al.[34] This explanation is supported by the surface Pt/Co molar ratio obtained from XPS. As shown in Table 1, nearly all the surface Pt/Co molar ratios of

Table S2. For the conventional heat prepared sample (i.e., Pt$_1$Co$_2$-con), there were two peaks for the Co species. The smaller peak, at 315 °C, can be ascribed to the reduction of Co$_3$O$_4$ to CoO, while the larger peak, at 385 °C, can be ascribed
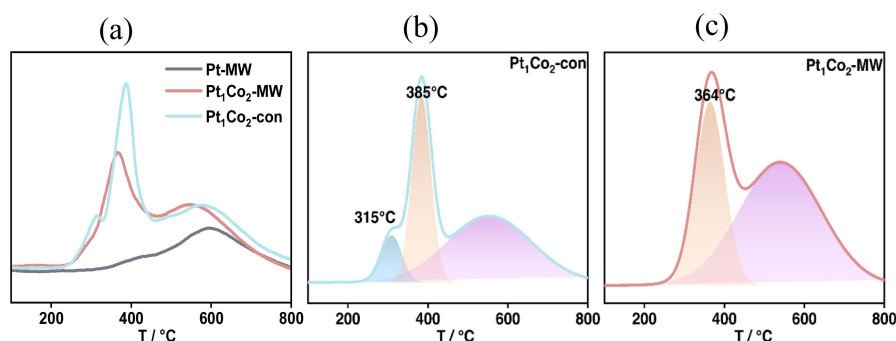
Figure 3. (a) H$_2$-TPR profiles of Pt-MW, Pt$_1$Co$_2$-MW, and Pt$_1$Co$_2$-con; Deconvolution of H$_2$-TPR profiles for (b) Pt$_1$Co$_2$-con, and (c) Pt$_1$Co$_2$-MW samples.

Table 1. ICP-OES results and surface Pt/Co ratios for the prepared samples.

Sample ID	Pt[a]/wt.%	Co[a]/wt.%	Metal/wt.%[b]	Pt/Co[c]	Pt/Co[e]
Pt-MW	2.40(5.00)	0.00(0.00)	2.40	–	–
Co-MW	0.00(0.00)	4.92(5.00)	4.32	0	0
Pt$_2$Co$_1$-MW	3.25(4.34)	0.76(0.66)[d]	4.01	1.30(2.00)	2.81(2.00)
Pt$_3$Co$_1$-MW	3.48(4.54)	0.65(0.46)[d]	4.13	1.64(3.00)	4(3.00)
Pt$_1$Co$_3$-MW	2.43(2.62)	2.23(2.38)	4.65	0.32(0.33)	0(0.33)
Pt$_1$Co$_2$-MW	2.45(3.12)	1.95(1.88)[d]	4.40	0.38(0.50)	1.94(0.50)
Pt$_1$Co$_2$-con	2.96(3.12)	1.91(1.88)[d]	4.87	0.47(0.50)	2.27(0.50)
Pt$_1$Co$_2$-2 m	1.76(3.12)	1.61(1.88)	3.38	0.33(0.50)	1.41(0.50)
Pt$_1$Co$_2$-6 m	2.46(3.12)	1.80(1.88)	4.26	0.41(0.50)	2.06(0.50)
Pt$_{10}$Co$_{10}$	2.90(3.12)	2.02(1.88)[d]	4.93	0.43(0.50)	3.03(0.50)
Pt$_{10}$Co$_2$	2.43(3.12)	1.66(1.88)	4.09	0.44(0.50)	0(0.50)
Co$_{10}$Pt$_{10}$	2.61(3.12)	2.06(1.88)[d]	4.67	0.38(0.50)	2.72(0.50)
Co$_{10}$Pt$_2$	1.72(3.12)	2.03(1.88)[d]	3.76	0.26(0.50)	1.17(0.50)
Pt$_1$Co$_2$-Used	2.41(3.12)	1.88(1.88)	4.29	0.39(0.50)	1.96(0.50)

Note: a) Nominal Pt and Co content in parentheses, calculated from the molar ratios of precursors. b) Total metal content of (Pt + Co) wt.%. c) Nominal Pt/Co molar ratio in parentheses, calculated from the molar ratios of precursors. d) The higher than nominal value was caused by the easier reduction of Co precursor. e) Surface Pt/Co molar ratio determined from XPS.

the PtCo bimetallic catalysts were higher than the nominal values (except for the Pt$_1$Co$_3$-MW and Pt$_{10}$Co$_2$ samples, due to their high Co content). These high ratio values are quite different from the bulk Pt/Co molar ratios. Co(acac)$_3$ was first reduced to Co^0, then Pt(acac)$_2$ and Co(acac)$_3$ co-deposited on the surface of the Co^0. Because most of the Co(acac)$_3$ was reduced in the initial stage, Pt was higher than Co during the co-deposition stage, leading to a higher surface Pt/Co molar ratio.

XPS was used to analyze the surface electronic properties of Pt, and the Pt 4f spectra are shown in Figure 4. There were two pairs of doublets, with the more intense doublet (71.34 eV and 74.65 eV) belonging to metallic Pt^0 and the other doublet (72.65 eV and 75.81 eV) corresponding to the Pt^{2+} chemical state.[35] Metallic Pt^0 comprised the majority of all the Pt content, and the existence of Pt^{2+} indicated that some Pt atoms were oxidized in the air. The 74.75% fraction of Pt^0 in Pt-MW increased to more than 75% when Co was alloyed with Pt. This
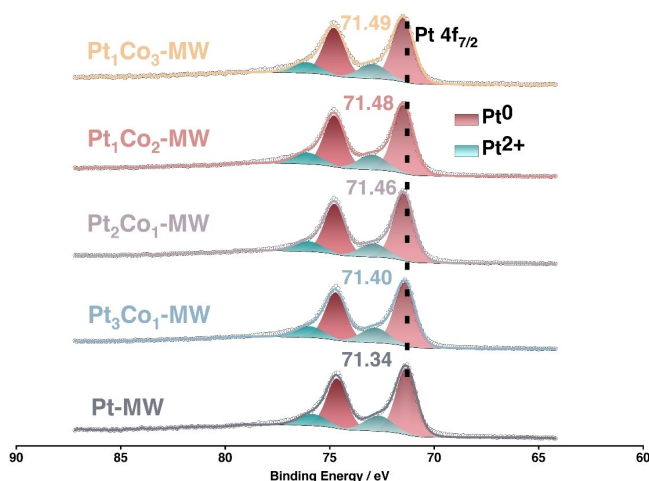
result was consistent with a previous report that the addition of Co enhanced the reduction of Pt^{2+}.[36] Binding energy (BE) is strongly related to the adsorption/desorption capability of the reaction species on the surface of the catalyst. The BE of Pt^0 in Pt-MW shifted positively from 71.34 eV to 71.40 eV with the addition of Co. It increased further as more Co was added. The positive shift in BE indicated an electron loss by Pt to Co, which is a hallmark of the alloying effect of Co on Pt.[37] However, this trend conflicted with the electronegativity of Pt (2.28) and Co (1.88). According to the electronegativity difference between Pt and Co, electrons should transfer from Co to Pt, lowering the BE of Pt^0.[38] A possible explanation was posed by Mukerjee et al.,[39] who used in situ XANES to investigate the 5d electron loss of Pt in Pt alloys (PtCr, PtCo, PtFe, and PtNi). Moreover, based on theoretical research, when the platinum atom is alloyed with the second component, the total number of electrons per platinum atom increases, while the 5d electrons decrease.[40] The confirmation of electron transfer direction was also achieved by examining the Co 2p spectrum, as depicted in Figure S2. The BEs at 780.6 eV and 796.3 eV were assigned to the Co 2p$_{3/2}$ and Co 2p$_{1/2}$ peaks, respectively.[41] Additionally, the BEs of two shakeup satellites (referred to as "Sat.") at 784.8 eV and 803.7 eV were observed, indicating the presence of Co with different oxidation states. In the Co-MW sample, the BE of Co 2p3/2 was 780.65 eV. However, with the alloy of Pt, the BE shifted to 780.05 eV in the negative direction.

Catalyst performance

Effects of MW time

The MW time greatly affected CAL conversion and COL selectivity. As can be seen from Figure 5, Pt$_1$Co$_2$-2 m showed the lowest CAL conversion and COL selectivity among the MW-prepared samples, possibly because of the low concentration of Pt and low surface Pt/Co ratio in the initial stage. With more MW time, more Pt was generated, and the CAL conversion and
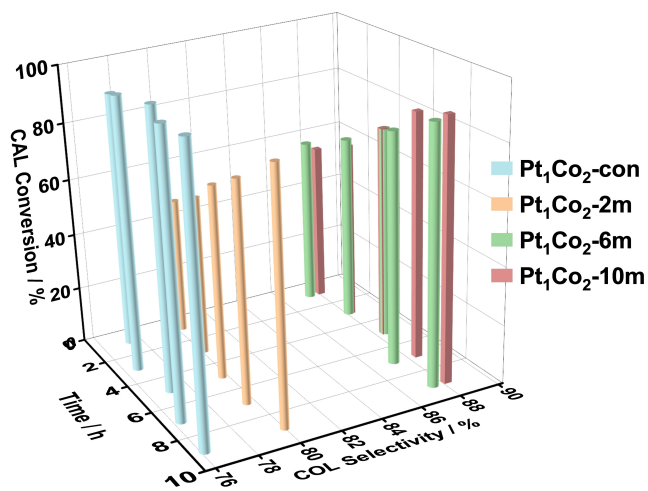

Figure 4. XPS spectra of MW-prepared Pt and PtCo alloy nanoparticle catalysts.

Figure 5. Effects of MW time on CAL conversion and COL selectivity.

Figure 6. Effects of Pt/Co ratio on CAL conversion and COL selectivity.

COL selectivity also increased. The highest CAL conversion and COL selectivity were obtained from the Pt_1Co_2-10 m sample. We also compared the performance of MW-prepared samples with the sample prepared by the conventional heat method (Pt_1Co_2-con), which showed a higher CAL conversion because of its higher Pt content (2.96 wt.%) and high surface Pt/Co ratio (2.27). But its COL selectivity was only 76%, much lower than that obtained from the Pt_1Co_2-10 m sample (89%). This difference could have resulted from weaker interaction between Pt and Co in the Pt_1Co_2-con sample, as confirmed by H_2-TPR results. Thus, to achieve high catalytic performance and save time, an MW time of 10 min was chosen for preparing PtCo alloy.

Effects of Pt/Co ratios

The effects of Pt/Co ratios on CAL conversion and COL selectivity were investigated. The Co- only sample with 4.92 wt.% of Co exhibited 10% CAL conversion and 85% COL selectivity after 9 h (not shown here), which meant the Co monometallic catalyst showed the lowest activity, consistent with previous reports.[24–25] The Pt-only sample showed the lowest COL selectivity, 64%. As shown in Figure 6, the introduction of Co significantly enhanced both CAL conversion and COL selectivity. All the PtCo alloy catalysts demonstrated a COL selectivity higher than 75%. Among these, the Pt_1Co_2-MW sample achieved the highest COL selectivity, 88%, with a CAL conversion of 90%. Also, the COL selectivity stayed nearly the same during the whole reaction time. The trend of bulk Pt/Co ratios was the same as the surface Pt/Co ratios, following the order Pt_3Co_1-MW $>$ Pt_2Co_1-MW $>$ Pt_1Co_2-MW $>$ Pt_1Co_3-MW, which was also the order of CAL conversions for different catalysts. The significant enhancements in CAL conversion and COL selectivity for the PtCo alloy catalysts can be ascribed to the synergistic effects between Pt and Co. The change of Pt electron properties with the addition of Co (as confirmed by
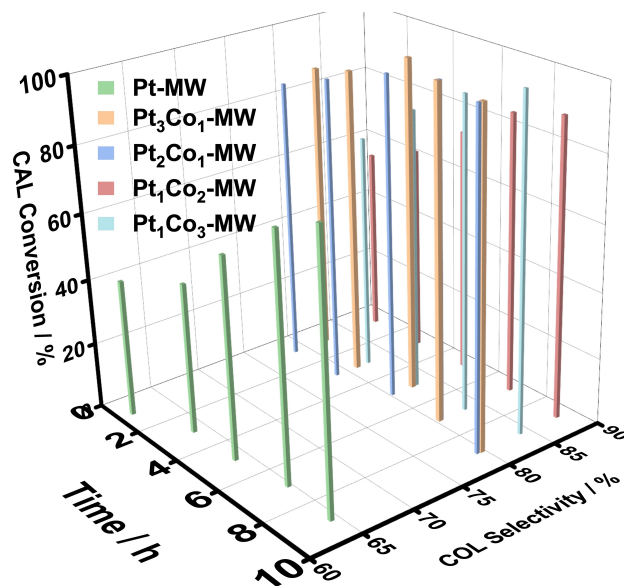
XPS) altered the adsorption model of CAL on the surface of the catalyst. The electrophilic Pt site favored the adsorption of the C=O bond through the lone-pair electrons of its oxygen atom. Therefore, the PtCo alloy catalysts outperformed the Pt monometallic catalyst during CAL hydrogenation, in terms of COL selectivity.

Effects of deposition sequence

The deposition sequence also had significant effects on the CAL conversion and COL selectivity. Our initial plan was to make a core-shell structure catalyst by changing the sequence of precursors, similar to the work reported by Sobal et al.[42] However, the core-shell structure formed at a relatively low temperature ($\sim 140\,°C$). The MW-assisted prepration operated at a higher temperature ($\sim 197\,°C$), causing the formation of PtCo alloy, not a core-shell structure. This finding was consistent with the results reported by Hsieh et al.[43] In their research, only PtCo alloy was obtained from a two-step MW-assisted method, no matter whether Pt or Co was deposited first, Nonetheless, we noted some useful information. For example, the CAL conversion, shown in Figure 7, followed the order of $Pt_{10}Co_2 <$ $Co_{10}Pt_2 < Pt_1Co_2$-10 m $< Co_{10}Pt_{10} < Pt_{10}Co_{10}$, which is also the order of surface Pt/Co ratios. Further, $Co_{10}Pt_{10}$ and $Pt_{10}Co_{10}$ showed higher CAL conversions, possibly because the longer MW time during catalyst preparation yielded higher Pt and Co contents and higher Pt/Co ratios on the catalyst surface. It was also interesting to note that $Co_{10}Pt_2$ showed a higher CAL conversion than $Pt_{10}Co_2$, although $Co_{10}Pt_2$ had a lower Pt and total metal content than $Pt_{10}Co_2$. The reason could be the higher surface Pt/Co ratio in $Co_{10}Pt_2$, whereas nearly all the Pt was covered by Co in $Pt_{10}Co_2$. Regarding COL selectivity, Pt_1Co_2-10 m prepared by co-adding $Pt(acac)_2$ and $Co(acac)_3$ as the
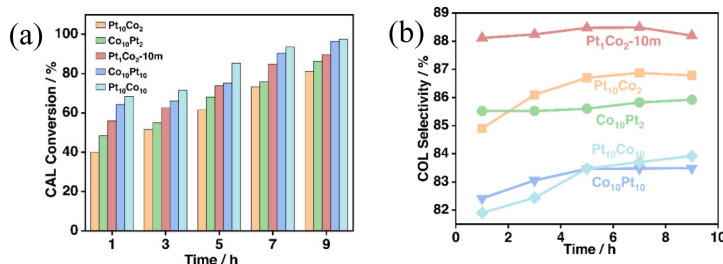
Figure 7. Effects of deposition sequence on (a) CAL conversion and (b) COL selectivity.

starting materials gave the highest selectivity. Among the sequentially added samples, the samples with Co(acac)₃ added later, such as $Pt_{10}Co_2$ and $Pt_{10}Co_{10}$, showed slightly higher COL selectivity than samples with Co(acac)₃ added first, such as $Co_{10}Pt_2$ and $Co_{10}Pt_{10}$. Therefore, co-adding Pt(acac)₂ and Co-(acac)₃ was chosen as the preferred method in preparing PtCo bimetallic catalysts.

Effects of reaction pressure

In CAL hydrogenation, higher hydrogen pressure causes more molecular hydrogen to dissolve in the solvent, which can increase the mass transfer and adsorption of hydrogen on active sites. Typically, liquid-phase hydrogenation follows a positive reaction order with respect to hydrogen partial pressure. In this study, as expected, CAL conversion increased as the hydrogen pressure increased from 5 bar to 20 bar, for

both Pt-MW and Pt_1Co_2-MW samples. Similar trends have been reported for many liquid hydrogenation reactions.[44–46] For example, on an unsupported Pt-based nanocrystal, a steady increase in CAL conversion from 21.6% at 1.5 bar to 83% at 10 bar was observed, and a stable value was reached at about 20 bar.[46] The increased conversion was attributed to enhanced mass transfer at higher pressure.[47] For COL selectivity, Pt-MW and Pt_1Co_2-MW behaved completely differently, as shown in Figure 8. For the monometallic Pt-MW sample, COL selectivity increased as hydrogen pressure increased from 5 bar to 20 bar. Similar results were reported by Lee et al., who found selectivity to COL was boosted when the hydrogen pressure increased from 1 bar to 10 bar, using 2% Pt/SBA-15 as the catalyst.[44] Possibly, surface crowding caused by increased hydrogen promoted the vertical adsorption mode of the C=O bond.[48] The Pt_1Co_2-MW sample had 100% COL selectivity at 5 bar, but when the pressure was increased to 10 bar and then to 20 bar, the COL selectivity dropped to around 85%. The introduction of Co significantly improved the selectivity by adjusting the Pt electronic structure. To further elucidate the different behaviors of Pt-MW and Pt_1Co_2-MW, we studied the hydrogenation of mixtures containing equivalent semi-hydrogenated products, such as HCAL (having only a C=O double bond) and COL (containing only a C=C double bond). The correlation between $\ln(C_0/C_t)$ and the reaction time (t) was established to evaluate the kinetic behaviors. C_0 represented the initial molar concentration of COL or HCAL, while C_t represented the molar concentration of COL or HCAL, which varied with reaction time. The COL hydrogenation rate can be used to quantify the rate of C=C bond hydrogenation, $k_{C=C}$, while the HCAL hydrogenation rate can be used to quantify the rate of C=O bond hydrogenation, $k_{C=O}$. The Pt_1Co_2-MW sample showed a much higher
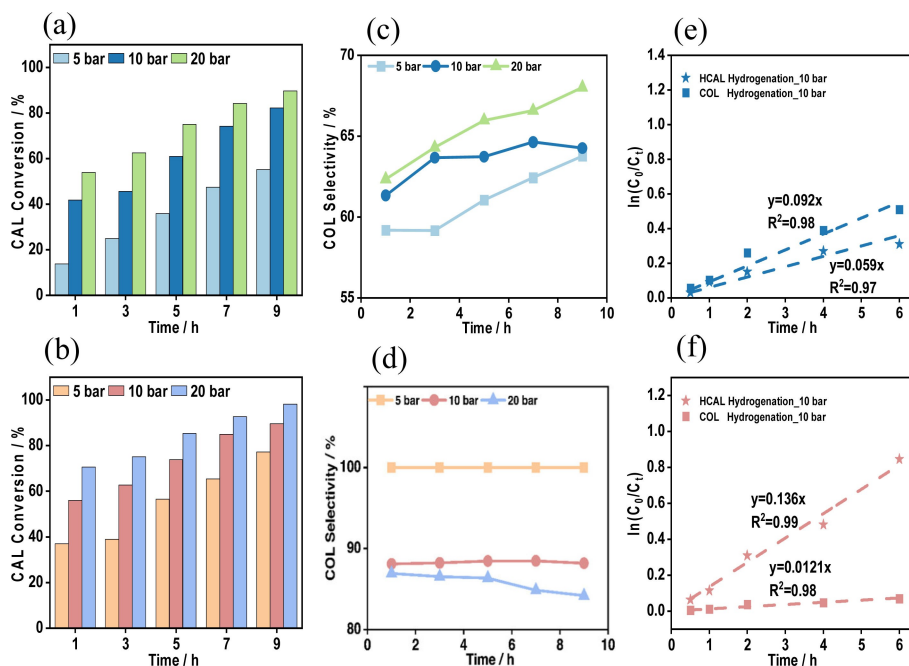

Figure 8. Effects of hydrogen pressure on CAL conversion using (a) Pt-MW and (b) Pt_1Co_2-MW samples; effects of hydrogen pressure on COL selectivity using (c) Pt-MW and (d) Pt_1Co_2-MW samples; $k_{C=O}/k_{C=C}$ ratios for (e) Pt-MW and (f) Pt_1Co_2-MW samples.

value of $k_{C=O}/k_{C=C}$ (11.2) than the Pt-MW sample (0.64), due to its preferential adsorption of the C=O bond.

Stability of the catalysts

The stability of catalysts is particularly important in their practical applications. For this reason, we investigated the stability of the most promising Pt_1Co_2-MW sample in CAL hydrogenation. After each reaction, the catalyst was washed three times with 2-propanol and collected by centrifugation. The obtained catalyst was then used for the next run under the same reaction conditions. As shown in Figure 9, only a negligible decrease in the conversion of CAL was observed, indicating good stability of the Pt_1Co_2-MW catalyst. To our surprise, the selectivity for COL increased slightly during the recycling experiments. The excellent stability of the catalyst can be attributed to the strong interaction between the support and the PtCo alloy. In our previous research, part of the PtCo on nonfunctional MWCNTs leached during the reaction, leading to lower performance after five cycles of experiments.[24] In this study, MWCNTs-COOH were used as the support, and they provided sufficient functional groups to anchor the PtCo NPs. The high energy of the MW method also contributed to the strong interaction between the support and the metal species. As shown in Figure S1, the average particle size of the spent catalyst was 8.8 ± 1.2 nm, which is slightly larger than that of fresh catalyst. This difference may explain why the COL selectivity increased slightly, because a large particle size is favorable for C=O bond hydrogenation. No segregation of Pt and Co was observed from EDS mapping of the spent sample. Also, based on the ICP-OES results in Table 1, the spent catalyst had negligible metal loss. To further illustrate the stability, the catalyst was filtered out after 3 h of reaction and the remaining system continued to react, but almost no CAL conversion was observed after the catalyst was removed. This finding indicates negligible metal leaching during the reaction, ensuring the performance of the catalysts under practical reaction conditions.
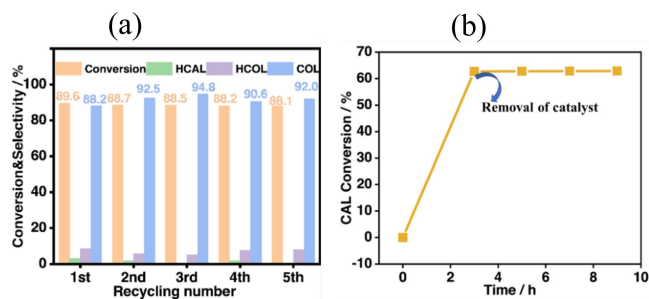
Discussion

The MW-heated preparation of PtCo alloy was conducted in an open reaction system under atmospheric pressure. Compared to preparation in a closed reaction system, MW-assisted preparation in an open reaction system is relatively simple, safe, and low-cost. The interaction between Pt and Co was stronger in the MW-prepared samples than in conventional heat-prepared samples. Pt_1Co_2-MW had a higher COL selectivity than Pt_1Co_2-con, indicating the advantages of using the MW method. Due to its sensitivity to electronic and geometric structure, the selective hydrogenation of α, β-unsaturated aldehydes was a model reaction for testing the obtained catalysts. To that end, the major strategies to improve the selectivity for unsaturated alcohol include confinement and electronic surface modification.[48]

We chose the electronic modification approach. Pt and Pt alloys have been widely used in the hydrogenation of unsaturated aldehydes. Among these alloys, monometallic Pt catalysts usually show low selectivity for unsaturated alcohols, and, due to electron transfer, the promotion of Pt with a secondary metal can significantly enhance the selectivity for unsaturated alcohol. Generally, Fe- or Co-promoted Pt facilitates C=O hydrogenation, while Ni-promoted Pt facilitates C=C hydrogenation.[46] In this study, PtCo alloy was prepared through MW-assisted polyol synthesis. The obtained catalysts had an average size of 8.5 nm, and such a large particle has a higher selectivity for COL.[49] The reported particle size from the MW-assisted polyol synthesis method also varied because of different preparation conditions. For example, PtNi alloy nano-particles measuring 6.9 nm to 9.2 nm were obtained using pulse mode MW heating with a pulse duration of 200s (20 s on and 180 s off) for different numbers of pulses.[50] Temperature played a vital role during the preparation. Pt_3Co alloy nanoparticles with an average size of 2.3 nm were obtained at 145 °C in a microwave oven (Sineo, MAS-II, 600 W, 2.45 GHz).[9] PtCr alloy nanoparticles with a similar diameter (2.4 ± 0.7 nm) were prepared at 150 °C in a microwave oven.[51] Unfortunately, however, our current experimental setup cannot control the temperature, so the preparation temperature was controlled by the boiling point of the solvent (i.e., EG at 197 °C). The relatively large PtCo alloy showed excellent COL selectivity, which was consistent with previous research.[52] Richard et al. attributed the particle size effect to a directing effect of the phenyl group. They proposed that the phenyl group was repelled on a large metal surface and the C=O bond was tilted so that it was easily hydrogenated. In contrast, a small metal surface did not have a steric constraint, so both C=C and C=O were adsorbed. C=C was thermally favored, and the selectivity for COL decreased.

Besides the particle size effects, the addition of Co further improved the selectivity. In our case, the electron transfer from Pt to Co made the Pt sites electrophilic. C=O was then easily adsorbed on the Pt sites through the lone-pair electrons of its oxygen atom. It is worth mentioning that the electron transfer from Pt to Co was against the electronegativity difference between Pt (2.28) and Co (1.88): Normally, electrons transfer from Co to Pt. Still, much research regarding electron transfers

Figure 9. Catalytic performance in recycling and leaching test experiments.

from Pt to Co has been reported.[28,53–55] For example, Zhang et al. reported that the BE of Pt $4f_{7/2}$ in Pt-oCNTs shifted from 71.08 ev to 71.48 ev when Co was added.[55] The PtCo catalyst was prepared by a modified oleyamine reduction method at 230 °C. Also, Wang et al. reported that, compared to a pure Pt sample, all the studied PtCo catalysts with different Pt/Co ratios exhibited higher BE values of Pt $4f_{7/2}$.[53] These catalysts were prepared by a modified polyol synthesis. The exact reason for the different electron transfer directions was not clear, but it still indicates a strong interaction between Pt and Co. One possible explanation for the positive Pt $4f7/2$ shift in XPS spectra should be made by the difference in work function between pure Pt and the alloy as mentioned by Weinert et al.[56] Their research showed that the change of work function $\triangle\Phi$ also had an influence on the direction of charge transfer. For example, the direction of charge transfer was reversed when $\triangle\Phi$ changed from 0.6 eV to −0.2 eV for a Pt/Re(0001) system. In our case, the electron transfer from Pt to Co altered the adsorption model of CAL and enhanced the selectivity for COL. A possible reaction pathway is shown in Figure 10.
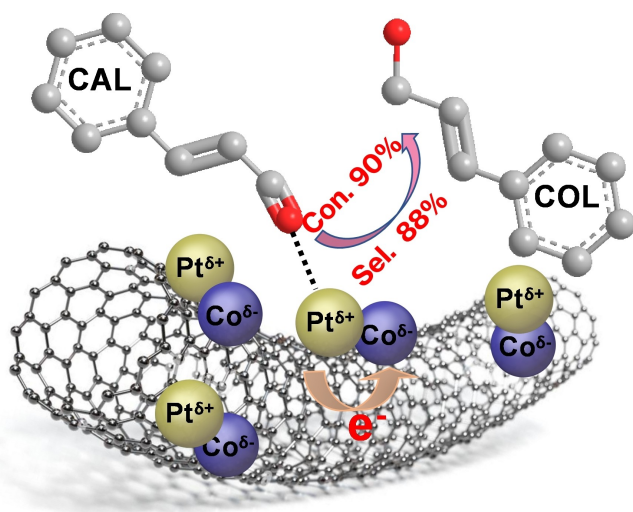

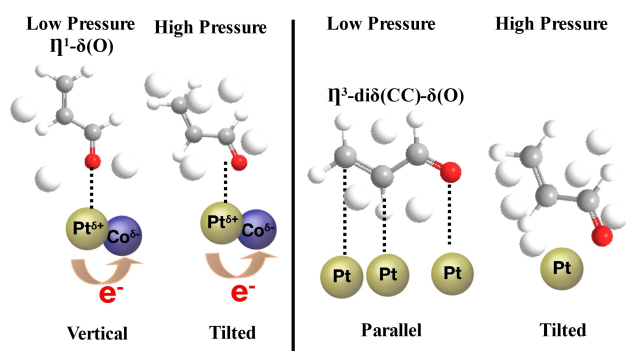**Figure 10.** A possible reaction pathway for CAL hydrogenation.

Figure 11. Changes in the adsorption model for Pt_1Co_2-MW (left) and Pt-MW (right) at low and high hydrogen pressure.

Hydrogen pressure played a vital role in COL selectivity. Pt_1Co_2-MW alloys and the Pt-MW monometallic catalyst showed quite different behaviors under different hydrogen pressures, possibly due to different adsorption models on the surfaces of the different catalysts. Typically, there are nine adsorption models for unsaturated aldehyde, as shown in Figure S3.[48] For the Pt_1Co_2-MW sample at a low pressure of 5 bar, the model has a vertical η^1-δ(O) configuration as shown in Figure 11. This configuration was caused by a change of the Pt electronic structure when Co was added, as mentioned previously. When the hydrogen pressure increased, the vertical adsorption was slightly tilted, leading to a decrease in COL selectivity. As for the Pt-MW sample, it had a parallel η^3-diδ(CC)-δ(O) configuration at a low pressure, with the C≡C bond binding more strongly than the C≡O bond.[48] The selectivity for COL was low at a low pressure of 5 bar. With increased hydrogen pressure, the catalyst surface became crowded, and the reactant hydrogen functioned as a surface ligand, tilting the adsorption of CAL away from vertical. Therefore, for the Pt-MW sample, the selectivity for COL increased as the hydrogen pressure increased, probably due to steric effects. To illustrate such steric effects, 1% Pt/ZIF-8 was prepared and tested for CAL hydrogenation. As shown in Figure S4, there was 100% selectivity for COL. However, the CAL conversion after 9 h was only 3.5%, due to the slow mass transfer. The small pore size of ZIF-8 allowed only the vertical adsorption of CAL. Thus, high hydrogen pressure can change the adsorption model on the Pt-MW surface, yielding higher selectivity for COL. Note that the above discussion is valid only for pressures between 5 to 20 bar.

Turnover frequency (TOF) was also calculated. The TOF value for CAL conversion was determined based on the number of surface-active Pt sites within the initial 15 min of reaction. A comparison of catalysts in this work with state-of-the-art catalysts in TOF value of CAL hydrogenation reaction is shown in Table S4. In our work, TOF value was increased as the surface Pt/Co surface ratio increased. For example, for the samples with Pt/Co surface ratio lower than 1.0, the TOF was 0.39 s^{-1} and 0.44 s^{-1} for Pt_1Co_2-MW and Pt_1Co_3-MW, respectively. When Pt/Co surface ratio was higher than 1.0, the TOF increased to 0.65 s^{-1} and 0.66 s^{-1} for Pt_3Co_1-MW and Pt_2Co_1-MW, respectively. A higher pressure can also lead to a higher TOF. For the Pt-MW sample, the TOF increased from 0.17 s^{-1} to 0.66 s^{-1} when the pressure increased from 5 bar to 20 bar. The same trend can also be observed in Pt_1Co_2-MW sample. The reported TOF value for PtCo catalysts ranged from 0.11 s^{-1} to 4.93 s^{-1} as listed in Table S4. The higher TOF may come from a smaller particle size. For the reported top Pt/CoAl-LDHs catalyst,[57] it had a particle size of 3.43 nm, which was much smaller than that in our catalyst. The support layered double hydroxides (LDHs) also contributed to the high TOF through electronic metal supported interaction. The comparison of performance between our catalyst and state-of-the-art catalysts has proven advantageous in our pursuit of advancing catalyst design. By conducting such comparative analyses, we were able to assess our catalyst in relation to established benchmarks.

Conclusions and Outlook

Five PtCo-supported catalysts were prepared with the assistance of MW heating for a few minutes. The MW-prepared samples all more selectively hydrogenated CAL than a sample prepared by conventional heating. The optimal Pt_1Co_2-MW catalyst achieved a COL selectivity of 88%, with a CAL conversion of 90%, while Pt_1Co_2-con had a COL selectivity of only 76%. Various characterizations revealed that the excellent performance of Pt_1Co_2-MW resulted from the strong interaction between Pt and Co. The alloyed Co adjusted the electronic structure of Pt, favoring the adsorption of the C=O bond. Moreover, the obtained alloy showed excellent stability, which is essential for practical applications. The high stability results from high energy of the MW irradiation and the abundance of functionalized groups on the support to anchor the metal species. Of course, there is still room to improve the performance. The effects of several factors, such as the heating style (pulse heating or continuous heating), solvents, and power level, on the catalytic performance could be further investigated.

Experimental section

Chemicals and materials

Cinnamaldehyde (CAL) (99.0 wt.%), hydrocinnamyl alcohol (HCOL) (98 wt.%), (cinnamyl alcohol) COL (98 wt.%), hydrocinnamaldehyde (HCAL) (>95%), 2-propanol (99.5%), toluene (99.85 wt.% for HPLC), EG (99.8 wt.%) were purchased from MilliporeSigma. Platinum(II) bis(acetylacetonate) $(Pt(acac)_2)$ (Pt>48.0 wt.%) and tris(acetylacetonato)cobalt(III) $(Co(acac)_3)$ (>98 wt.%) were obtained from Alfa Aesar, Inc. Functionalized MWCNTs (MWCNTs-COOH, >95%, stock #US4311) were purchased from US Research Nanomaterials, Inc.

Microwave assisted polyol synthesis of Pt based catalysts

In a typical synthesis, appropriate amounts of $Pt(acac)_2$ and $Co(acac)_3$ as well as MWCNTs-COOH were mixed in 50 mL of EG in a three-necked flask under vigorous stirring. Nitrogen (N_2) was bubbled into the mixture for 30 min to flush out air. Then, the three-necked flask was transferred to the microwave reactor and the reaction was initialed by setting the output power to 600 W. Mechanical stirring was used to achieve uniform microwave irradiation, and the whole process was conducted in an N_2 atmosphere. A reflux system was attached to the open circular flask of the MW system to allow condensation of the solvent by reflux. After it cooled to room temperature (in about 10 min), the mixture was removed. The solids were collected by filtration and washed thoroughly with warm deionized (DI) water and ethanol for three times each, followed by a vacuum drying. The designed total metal content was 5 wt.%. The obtained catalyst was denoted as Pt_xCo_y-MW, where x and y represent the molar ratio of $Pt(acac)_2$ and $Co(acac)_3$ in the initial solution. For example, Pt_1Co_2-MW means the molar ratio of $Pt(acac)_2$ and $Co(acac)_3$ was 1:2 in the initial solution. The actual metal content was measured by inductively coupled plasma - optical emission spectrometry (ICP-OES). For the optimized Pt_1Co_2-MW catalyst, we also investigated the effects of the microwave time (2, 6, and 10 min) at 600 W. The resulting catalysts were denoted as Pt_1Co_2-2 m, Pt_1Co_2-6 m, and Pt_1Co_2-10 m, respectively. We also investigated the effects of the metal deposition sequence on the optimized Pt_1Co_2-MW catalyst. For this purpose, $Pt(acac)_2$ or $Co(acac)_3$ was first reduced for 10 min, then

$Co(acac)_3$ or $Pt(acac)_2$ was added to the mixture for 2 or 10 min. The resulting catalysts were denoted as $Pt_{10}Co_2$, $Pt_{10}Co_{10}$, $Co_{10}Pt_2$, and $Co_{10}Pt_{10}$, respectively. Here, $Pt_{10}Co_2$ means that $Pt(acac)_2$ was first reduced for 10 min, then $Co(acac)_3$ was added for another 2 min of reduction.

For comparison, a catalyst was also prepared by conventional polyol synthesis (i.e., heating at reflux). In this method, $Pt(acac)_2$ and $Co(acac)_3$ in molar ratio of 1:2, along with MWCNTs-COOH, were mixed in 50 mL of EG, and N_2 was bubbled through the mixture for 30 min to flush out air. The synthesis reaction was conducted at ~197 °C in an oil bath for 1 h under vigorous stirring and the protection of N_2. The subsequent procedures were the same as in the MW-assisted process. The obtained catalyst was marked as Pt_1Co_2-con.

Catalyst characterizations

To evaluate the crystalline structure and particle size of Pt and Co NPs, morphology was performed using a FEI Talos F200X operated at 200 kV and equipped with a Super X energy-dispersive spectrometer (EDS). Scanning TEM (STEM) high-angle annular dark field (HAADF) images were used to highlight Pt and Co NPs with MWCNTs matrix in contrast. STEM-EDS mapping was performed to confirm the elemental species and distribution. X-ray diffraction (XRD) measurements were performed with a Philips X'Pert PRO PW3050 X-ray diffractometer equipped with Cu Kα radiation and a graphite generator in the 2θ range of 10–90°.

After the samples were digested in hot aqua regia solution, the mass contents of Pt and Co were obtained by ICP-OES. X-ray photoelectron spectroscopy (XPS) was used to verify the formation of the bimetallic structure of the PtCo catalyst. XPS spectra were recorded with a Kratos Axis 165 X-ray photoelectron spectrometer, using monochromatic Al Ka radiation.

H_2 temperature-programmed reduction (H_2-TPR) was performed by employing 150 mg of sample in each measurement, using a Micromeritics Autochem II 2920 equipped with a thermal conductivity detector (TCD). First, the samples were pretreated with argon at 300 °C for 1 h (heating rate of 10 °C/min). Then, the sample was cooled to 100 °C in a stream of argon gas at a flow rate of 30 mL/min. Finally, the temperature was increased to 800 °C at a rate of 10 °C/min under 10% H_2 in the argon gas stream.

Hydrogenation of CAL

The liquid-phase hydrogenation reaction was conducted in a 50 mL stainless steel Parr reactor loaded with 50 mg of the catalysts, 30 mL of 2-propanol, and 0.5 g of CAL. The reactor was flushed 6 times with 10 bar H_2 to drive air out of the reactor at room temperature. Then the reactor was pressurized with H_2 to the desired pressure. The reaction was carried out at 80 °C for 9 h, with stirring at 800 rpm to eliminate mass transfer resistance.[25] During the reaction, approximately 1 mL of sample was taken periodically and quantified by gas chromatography (GC, Agilent 6890), using toluene as an internal standard. In cyclic experiments, the catalyst was washed with 2-propanol three times and collected by centrifugation. For the leaching test, the catalyst was filtered out after 3 h of reaction. The remaining system continued to react for another 6 h without the catalyst. Samples were collected and analyzed at one-hour intervals to monitor the change of CAL.

[1] W. Yu, M. D. Porosoff, J. G. Chen, *Chem. Rev.* **2012**, *112*, 5780–5817.

[2] J. E. S. van der Hoeven, J. Jelic, L. A. Olthof, G. Totarella, R. J. A. Van Dijk-Moes, J. M. Krafft, C. Louis, F. Studt, A. Van Blaaderen, P. E. De Jongh, *Nat. Mater.* **2021**, *20*, 1216–1220.

[3] W. U. Khan, L. Baharudin, J. Choi, A. C. K. Yip, *ChemCatChem* **2020**, *13*, 111–120.

[4] L. Xie, J. Liang, C. Priest, T. Wang, D. Ding, G. Wu, Q. Li, *Chem. Commun.* **2021**, *57*, 1839–1854.

[5] S. He, Y. Liu, H. Zhan, L. Guan, *ACS Catal.* **2021**, *11*, 9355–9365.

[6] L. Pavko, M. Gatalo, G. Krizan, J. Krizan, K. Ehelebe, F. Ruiz-Zepeda, M. Sala, G. Drazic, M. Geuss, P. Kaiser, M. Bele, M. Kostelec, T. Dukic, N. Van de Velde, I. Jerman, S. Cherevko, N. Hodnik, B. Genorio, M. Gaberscek, *ACS Appl. Energ. Mater.* **2021**, *4*, 13819–13829.

[7] M. K. Kabiraz, B. Ruqia, J. Kim, H. Kim, H. J. Kim, Y. Hong, M. J. Kim, Y. K. Kim, C. Kim, W.-J. Lee, W. Lee, G. H. Hwang, H. C. Ri, H. Baik, H.-S. Oh, Y. W. Lee, L. Gao, H. Huang, S. M. Paek, Y.-J. Jo, C. H. Choi, S. W. Han, S.-I. Choi, *ACS Catal.* **2022**, *12*, 3516–3523.

[8] C. Li, C. Ke, R. Han, G. Fan, L. Yang, F. Li, *J. Mol. Catal.* **2018**, *455*, 78–87.

[9] J. Shi, R. Nie, M. Zhang, M. Zhao, Z. Hou, *Chin. J. Catal.* **2014**, *35*, 2029–2037.

[10] B. Wu, H. Huang, J. Yang, N. Zheng, G. Fu, *Angew. Chem. Int. Ed. Engl.* **2012**, *51*, 3440–3443.

[11] C. Wang, H. Daimon, T. Onodera, T. Koda, S. Sun, *Angew. Chem. Int. Ed. Engl.* **2008**, *120*, 3644–3647.

[12] J. Wu, J. Zhang, Z. Peng, S. Yang, F. T. Wagner, H. Yang, *J. Am. Chem. Soc.* **2010**, *132*, 4984–4985.

[13] S. I. Choi, R. Choi, S. W. Han, J. T. Park, *Chemistry* **2011**, *17*, 12280–12284.

[14] Z. Zhou, S. Wang, W. Zhou, G. Wang, L. Jiang, W. Li, S. Song, J. Liu, G. Sun, Q. Xin, *Chem. Commun.* **2003**, 394–395.

[15] F. Fievet, S. Ammar-Merah, R. Brayner, F. Chau, M. Giraud, F. Mammeri, J. Peron, J. Y. Piquemal, L. Sicard, G. Viau, *Chem. Soc. Rev.* **2018**, *47*, 5187–5233.

[16] A. G. R. Howe, R. Maunder, D. J. Morgan, J. K. Edwards, *Catalysts* **2019**, *9*.

[17] T. C. Deivaraj, W. Chen, J. Y. Lee, *J. Mater. Chem.* **2003**, *13*.

[18] Q. Chen, T. Ma, F. Wang, Y. Liu, S. Liu, J. Wang, Z. Cheng, Q. Chang, R. Yang, W. Huang, L. Wang, T. Qin, W. Huang, *Adv. Sci.* **2020**, *7*, 2000480.

[19] S. Komarneni, D. Li, B. Newalkar, H. Katsuki, A. S. Bhalla, *Langmuir* **2002**, *18*, 5959–5962.

[20] M. Tsuji, M. Kubokawa, R. Yano, N. Miyamae, T. Tsuji, M. S. Jun, S. Hong, S. Lim, S. H. Yoon, I. Mochida, *Langmuir* **2007**, *23*, 387–390.

[21] A. B. A. A. Nassr, I. Sinev, M.-M. Pohl, W. Grünert, M. Bron, *ACS Catal.* **2014**, *4*, 2449–2462.

[22] M. Tsuji, K. Uto, T. Nagami, A. Muto, H. Fukushima, J.-i. Hayashi, *ChemCatChem* **2017**, *9*, 962–970.

[23] A. Nurudeen Adewunmi, S. Akindeji Jerome, S. Huaneng, K. Lindiwe Eudora, in *Electrocatalysis and Electrocatalysts for a Cleaner Environment - Fundamentals and Applications* (Ed.: L. Khotseng), **2022**.

[24] X. Wang, Y. He, Y. Liu, J. Park, X. Liang, *J. Catal.* **2018**, *366*, 61–69.

[25] K. Wang, X. He, J. C. Wang, X. Liang, *Nanotechnology* **2022**, *33*, 215602.

[26] J. Safari, S. Gandomi-Ravandi, *J. Mol. Struct.* **2014**, *1074*, 71–78.

[27] D. Kaewsai, P. Piumsomboon, K. Pruksathorn, M. Hunsom, *RSC Adv.* **2017**, *7*, 20801–20810.

[28] H. Huang, X. Hu, J. Zhang, N. Su, J. Cheng, *Sci. Rep.* **2017**, *7*, 45555.

[29] W. Diao, J. M. M. Tengco, J. R. Regalbuto, J. R. Monnier, *ACS Catal.* **2015**, *5*, 5123–5134.

[30] T. R. Garrick, W. Diao, J. M. Tengco, E. A. Stach, S. D. Senanayake, D. A. Chen, J. R. Monnier, J. W. Weidner, *Electrochim. Acta* **2016**, *195*, 106–111.

[31] A. K. Hill, L. Torrente-Murciano, *Appl. Catal. B* **2015**, *172–173*, 129–135.

[32] H. Zhang, C. Lancelot, W. Chu, J. Hong, A. Y. Khodakov, P. A. Chernavskii, J. Zheng, D. Tong, *J. Mater. Chem.* **2009**, *19*.

[33] A. Tavasoli, K. Sadagiani, F. Khorashe, A. A. Seifkordi, A. A. Rohani, A. Nakhaeipour, *Fuel Process. Technol.* **2008**, *89*, 491–498.

[34] J.-H. Jang, J. Kim, Y.-H. Lee, I. Y. Kim, M.-H. Park, C.-W. Yang, S.-J. Hwang, Y.-U. Kwon, *Energy Environ. Sci.* **2011**, *4*, 4947–4953.

[35] C.-T. Hsieh, Y.-Y. Liu, W.-Y. Chen, Y.-H. Hsieh, *Int. J. Hydrogen Energy* **2011**, *36*, 15766–15774.

[36] A. S. Aricò, A. K. Shukla, H. Kim, S. Park, M. Min, V. Antonucci, *Appl. Surf. Sci.* **2001**, *172*, 33–40.

[37] S. Hidai, M. Kobayashi, H. Niwa, Y. Harada, M. Oshima, Y. Nakamori, T. Aoki, *J. Power Sources* **2011**, *196*, 8340–8345.

[38] N. Jung, S. Bhattacharjee, S. Gautam, H.-Y. Park, J. Ryu, Y.-H. Chung, S.-Y. Lee, I. Jang, J. H. Jang, S. H. Park, D. Y. Chung, Y.-E. Sung, K.-H. Chae, U. V. Waghmare, S.-C. Lee, S. J. Yoo, *NPG Asia Mater.* **2016**, *8*, e237-e237.

[39] S. Mukerjee, S. Srinivasan, M. P. Soriaga, J. McBreen, *J. Electrochem. Soc.* **1995**, *142*, 1409–1422.

[40] M. Wakisaka, S. Mitsui, Y. Hirose, K. Kawashima, H. Uchida, M. Watanabe, *J. Phys. Chem. B* **2006**, *110*, 23489–23496.

[41] D. Wu, Y. Wei, X. Ren, X. Ji, Y. Liu, X. Guo, Z. Liu, A. M. Asiri, Q. Wei, X. Sun, *Adv. Mater.* **2018**, *30*.

[42] N. S. Sobal, U. Ebels, H. Möhwald, M. Giersig, *J. Phys. Chem. B* **2003**, *107*, 7351–7354.

[43] C.-T. Hsieh, W.-Y. Chen, I. L. Chen, A. K. Roy, *J. Power Sources* **2012**, *199*, 94–102.

[44] L. J. Durndell, C. M. Parlett, N. S. Hondow, M. A. Isaacs, K. Wilson, A. F. Lee, *Sci. Rep.* **2015**, *5*, 9425.

[45] J. Breen, *Appl. Catal. A* **2004**, *268*, 267–274.

[46] W. O. Oduro, N. Cailuo, K. M. Yu, H. Yang, S. C. Tsang, *Phys. Chem. Chem. Phys.* **2011**, *13*, 2590–2602.

[47] V. Schettino, R. Bini, *Chem. Soc. Rev.* **2007**, *36*, 869–880.

[48] M. Luneau, J. S. Lim, D. A. Patel, E. C. H. Sykes, C. M. Friend, P. Sautet, *Chem. Rev.* **2020**, *120*, 12834–12872.

[49] S. C. Tsang, N. Cailuo, W. Oduro, A. T. Kong, L. Clifton, K. M. Yu, B. Thiebaut, J. Cookson, P. Bishop, *ACS Nano* **2008**, *2*, 2547–2553.

[50] R. Lin, X. Cai, Z. Hao, H. Pu, H. Yan, *Electrochim. Acta* **2018**, *283*, 764–771.

[51] N. E. Sahin, T. W. Napporn, L. Dubau, F. Kadirgan, J.-M. Léger, K. B. Kokoh, *Appl. Catal. B* **2017**, *203*, 72–84.

[52] A. Giroir-Fendler, D. Richard, P. Gallezot, *Catal. Lett.* **1990**, *5*, 175–181.

[53] Y. Zhao, J. Liu, Y. Zhao, F. Wang, *Phys. Chem. Chem. Phys.* **2014**, *16*, 19298–19306.

[54] X. Zhang, H. Wang, J. Key, V. Linkov, S. Ji, X. Wang, Z. Lei, R. Wang, *J. Electrochem. Soc.* **2012**, *159*, B270-B276.

[55] J. Su, W. Shi, X. Liu, L. Zhang, S. Cheng, Y. Zhang, G. A. Botton, B. Zhang, *J. Catal.* **2020**, *388*, 164–170.

[56] M. Weinert, R. E. Watson, *Phys. Rev. B* **1995**, *51*, 17168–17180.

[57] Z. Gao, L. Cai, C. Miao, T. Hui, Q. Wang, D. Li, J. Feng, *ChemCatChem* **2022**, *14*, e202200634.

RESEARCH ARTICLE

High selectivity toward C=O hydrogenation: PtCo alloy supported on MWCNTs-COOH was prepared within 10 minutes by a microwave irradiation. The electron transfer from Pt to Co made the Pt sites electrophilic, faciliting the adsorption of C=O functional group. As a result, a high selectivity toward cinnamyl alcohol was achieved in cinnamaldehyde hydrogenation reaction.
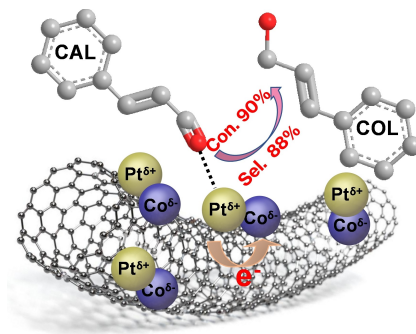
K. Wang, Dr. Y. Liu, Prof. Dr. J.-C. Wang, Prof. Dr. X. Liang*

1 – 11

PtCo/MWCNTs Prepared by a Microwave-assisted Polyol Method for Selective Cinnamaldehyde Hydrogenation